Prompt Chemistry of Alkenoxy Radical Products of the Double H-Atom Transfer of Alkoxy Radicals from Isoprene

Theodore S. Dibble*

Chemistry Department, State University of New York, College of Environmental Science and Forestry, Syracuse, New York 13210

Received: October 31, 2003; In Final Form: December 31, 2003

Quantum mechanical calculations have previously shown that certain second-generation alkoxy radicals formed in the atmospheric degradation of isoprene (2-methyl-1,3-butadiene) will undergo a novel reaction pathway: the simultaneous jumping of two H-atoms across the hydrogen bonds with a barrier of only ∼5 kcal/mol. The alkenoxy radical products of these double H-atom transfers are formed with ∼20−25 kcal/mol of energy, and may promptly decompose in competition with quenching to thermal energies. The fate of the energized alkenoxy radicals was determined under atmospheric and common laboratory conditions with use of stochastic Master equation analyses with relative energies determined at the B3LYP/6-311G(2df,2p) level of theory. The analyses accounted for the differing stabilities of, and interconversions between, conformers of the alkenoxy radicals with different numbers and arrangements of hydrogen bonds. Atmospheric implications of the double H-atom transfer are discussed.

Introduction

In a previous paper,[1] we demonstrated that certain second-generation alkoxy radicals formed in the atmospheric degradation of isoprene possess a fascinating hydrogen bonding motif involving two intramolecular OH- - -O hydrogen bonds. This structure permits a double intramolecular transfer of hydrogen atoms across the hydrogen bonds, in a single step, at rates which appear to dominate their atmospheric fates:

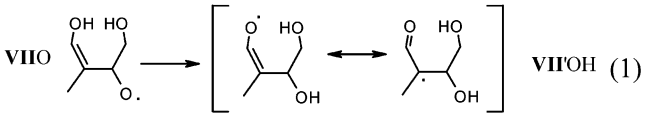

(1)

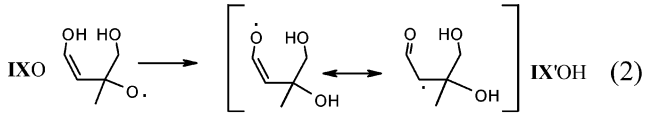

(2)

(the numbering of the radicals is kept consistent with that used in recent studies of isoprene chemistry). The present paper examines the fate of alkenoxy radicals **VII′**OH and **IX′**OH under conditions relevant to the atmosphere and to laboratory experiments. Reactions 1 and 2 are exothermic, so **VII′**OH and **IX′**OH are formed with significant internal energy. Their fate will initially be determined by competition between quenching and prompt decomposition, e.g.:

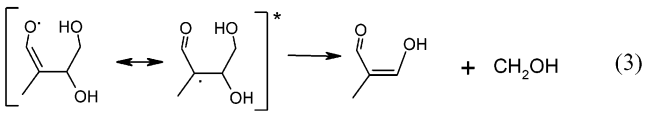

(3)

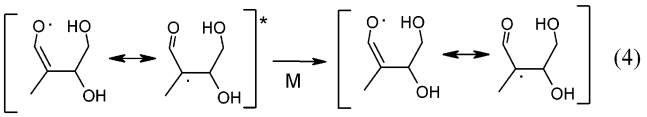

(4)

* Address correspondence to the author at the following: fax 315-470-6856; e-mail tsdibble@syr.edu.

Determination of the fate of **VII′**OH and **IX′**OH is not straightforward, because each may occur in multiple conformers with different numbers and arrangements of hydrogen bonds. Furthermore, the hydrogen-bonding arrangements affect the activation barriers for decomposition, so it is necessary to study each conformer and its activation barrier for decomposition.

The rest of the paper is organized as follows: first, the computational methods are described. The discussion then turns to the structure and energetics of the hydrogen-bonding arrangements in the alkenoxy radical products of the double H-atom transfer reactions. Results of simulations of the time-resolved kinetics are then presented, showing the effects of pressure and initial energy on the competition between prompt decomposition and stabilization of these alkenoxy radicals. Finally, we suggest reaction mechanisms likely to occur after the double H-atom transfer reactions, and evaluate the atmospheric consequences.

Computational Methods

Quantum chemical computations were carried out with the GAUSSIAN98[2] series of programs. Calculations used the hybrid exchange functional of Becke[3] and the correlation functional of Lee, Yang, and Parr,[4] a combination denoted B3LYP. Structures and harmonic vibrational frequencies of all species were obtained at B3LYP/6-31G(d,p). The vibrational frequencies were inspected to verify that transition states possessed only a single imaginary vibrational frequency. The structures of all species were re-optimized at B3LYP/6-311G(2df,2p). All radicals and transition states were treated with the spin-unrestricted formalism. Intrinsic reaction coordinate (IRC) calculations were carried out to verify the nature of some of the transition states, while the identities of other transition states were verified by inspection of their structure and the vector of the imaginary frequency.

The MultiWell program of Barker[5,6] was used to model the competition between the quenching and decomposition of the alkenoxy radicals produced from the double H-atom transfer of the alkoxy radicals. The MultiWell program uses a stochastic RRKM/Master Equation approach to determine the evolution

10.1021/jp0312161 CCC: $27.50
Published on Web 03/03/2004

of the energies and populations of the various species involved in the reaction. Simulations were run over time periods of picoseconds to microseconds at pressures of 10 and 760 Torr of N_2 at a variety of initial energies. Lennard-Jones parameters for the radicals were estimated by the method suggested by Gilbert and Smith[7] to be $\sigma = 6.26$ Å and $\epsilon = 500$ K. Energy-transfer parameters were chosen following the guidelines of Barker, Yoder, and King[8] to be $\alpha(E) = 40\ cm^{-1} + 0.025(E)$, where the probability of transfer of population from energy E to a lower energy E' is proportional to $\exp\{-(E - E')/\alpha(E)\}$. The number of Monte Carlo trials was set at 10 000 to provide a statistical uncertainty of 0.005 or less for the fraction of the population represented by each decomposition product or radical. Unscaled harmonic vibrational frequencies were used to determine the densities of states of reactants and transition states.

Results and Discussion

Structural parameters, activation barriers, and energies of reaction reported in the text are derived from B3LYP/6-311G(2df,2p) calculations (with zero-point energies calculated at 6-31G(d,p)) unless otherwise specified. Results from both basis sets are reported in the appropriate tables. The discussion of molecular structure focuses on hydrogen bonding, but Cartesian coordinates of the most important species may be found in the Supporting Information.

At this point we introduce the nomenclature we use to identify the particular hydrogen-bonding arrangements of the radicals. The carbon atoms numbered 1, 3, and 4 in the parent isoprene molecule are bonded to oxygen atoms in **VII′**OH (and **VII**O). In specifying the oxygen atoms participating in hydrogen bonding we use the number of the carbon atom to identify the oxygen atom. An arrow links the number representing the two oxygen atoms participating in a hydrogen bond; the arrow points from the oxygen donating the hydrogen atom to the oxygen atom accepting the hydrogen bond. Therefore, the doubly hydrogen bonded structure from which the double H-atom transfer occurs is labeled **VII**O(1→4,4→3). The product of the double H-atom transfer is therefore denoted **VII′**OH (3→4,4→1); this and other conformers of **VII′**OH are depicted in Figure 1. For purposes of numbering hydrogen bonding motifs, we treat **IX**O and **IX′**OH as isomers of **VII**O and **VII′**OH with the methyl group transposed to carbon 3.

A. Structure and Energetics of Alkenoxy Radicals. In (*Z*)-**VII′**OH (3→4,4→1) or (*Z*)-**IX′**OH (3→4,4→1), the two hydrogen bond distances in each radical are more nearly equal than those of (*Z*)-**VII**O (1→4,4→3) or (*Z*)-**IX**O (1→4,4→3) (compare Figure 1 to Figure 4 of ref 1). We investigated conformers for (*Z*)-**VII′**OH with zero, one, or two hydrogen bonds, as shown in Figure 1. Note that there exists a second doubly hydrogen-bonded conformer of **VII′**OH with a (4→3,3→1) arrangement of hydrogen bonds. Both doubly hydrogen-bonded conformers have hydrogen bonds donated in series from one site to the next. We also attempted to find potential energy minima for **VII′**OH-(4→1,3→1), that is, a structure with two hydrogen bonds donated to the same oxygen. However, proposed **VII′**OH-(4→1,3→1) structures tended to lose one of the hydrogen bonds during the geometry optimization.

As can be deduced from the relative energies listed in Table 1 and the potential energy profile shown in Figure 2, while the direction of the hydrogen bonding in **VII′**OH can be changed, the relative energy of the conformers is almost independent of the orientation of the hydrogen bonds. Loss of a hydrogen bond raises the energy of **VII′**OH by about 2 kcal/mol.

Transition states were found for the *E*/*Z* isomerization of the conformers with zero or one hydrogen bond; these transition state structures roughly correspond to 90° internal rotations about the C=C bond. The (*E*) isomers were found to be 1.5−1.9 kcal/mol higher in energy than the corresponding (*Z*) isomers, and as shown in Figure 2, the transition states for *E*/*Z* isomerization were rather high in energy. Model results indicated that the (*Z*) isomers of **VII′**OH either decompose or undergo conformational change much more rapidly than they undergo isomerization to the (*E*) forms. Therefore, the (*E*) isomers of **VII′**OH are of negligible importance under atmospheric conditions. While we identified the transition states for decomposition of the (*E*)

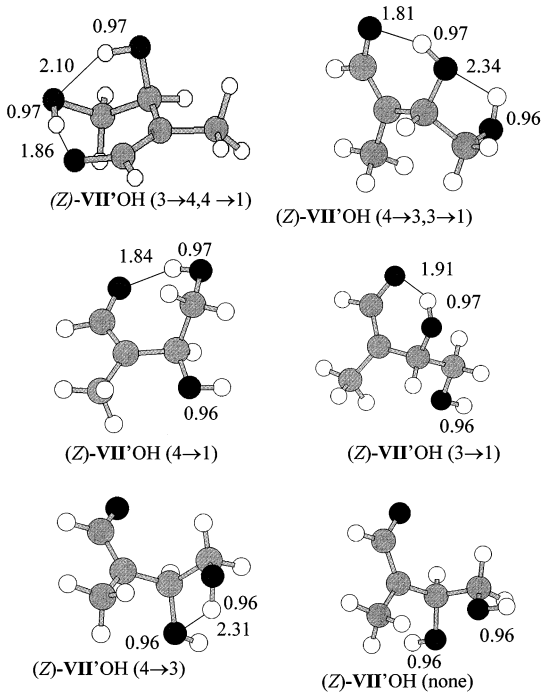

Figure 1. Structures of various conformers of alkenoxy radicals **VII′**OH. O−H distances (B3LYP/6-311G(2df,2p) values, in Å) are listed for covalent bonds and hydrogen bonds. Thin lines indicate hydrogen bonds.

TABLE 1: B3LYP Energies (kcal/mol) of VIIO, VII′OH, Their Conformers, Isomers, Exit Channel Complexes, and Decomposition Products, Relative to (*Z*)-VII′OH (3→4,4→1)

species	B3LYP/ 6-31G(d,p)	B3LYP/ 6-311G(2df,2p)
(*Z*)-**VII**O (1→4,4→3)	18.6	19.2
(*Z*)-**VII′**OH (3→4,4→1)	0.0	0.0
(*Z*)-**VII′**OH (4→3,3→1)	0.6	0.1
(*Z*)-**VII′**OH (3→1)	2.6	1.7
(*Z*)-**VII′**OH (4→1)	2.4	1.6
(*Z*)-**VII′**OH (4→3)	3.0	1.8
(*E*)-**VII′**OH (4→3)	4.8	3.5
(*Z*)-**VII′**OH (3→4)	2.9	1.5
(*E*)-**VII′**OH (3→4)	4.6	3.0
(*Z*)-**VII′**OH (none)	5.9	4.2
(*E*)-**VII′**OH (none)	7.4	5.6
exit channel complex from (*Z*)-**VII′**OH (4→3,3→1)[a]	12.7 (12.2)	9.9 (9.8)
exit channel complex from (*Z*)-**VII′**OH (4→1)[a]	17.4 (15.1)	13.6 (12.1)
exit channel complex from (*Z*)-**VII′**OH (4→3)[a]	19.5 (16.5)	15.4 (13.7)
3-hydroxy-2-methylpropenal (#2) + CH_2OH	17.9	14.7
3-hydroxy-2-methylpropenal (#3) + CH_2OH	26.6	22.2

[a] Numbers in parentheses give energies of exit channel complexes with respect to the specific conformer producing the complex.

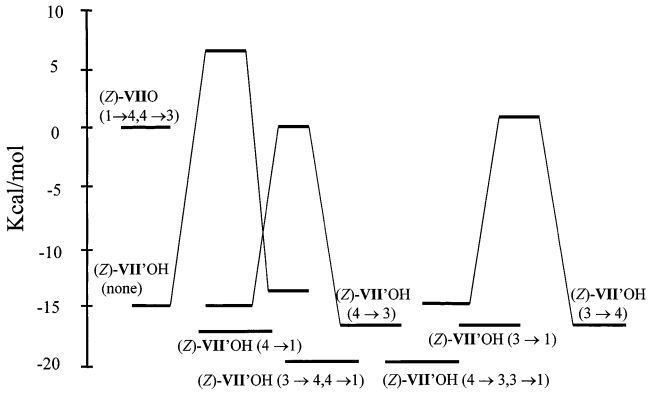

Figure 2. Relative energies of various conformers of **VII′**OH and potential energy profile for their *E*/*Z* isomerizations.

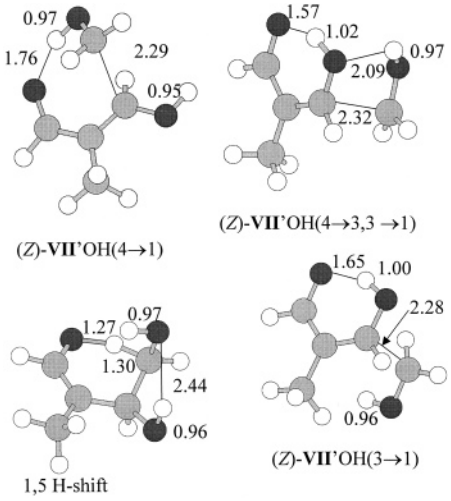

Figure 3. Structures of transition states for decomposition of **VII′**OH. Labels correspond to the conformer of the reactant. Distances (B3LYP/6-311G(2df,2p) values, in Å) are listed for covalent O−H bonds, hydrogen bonds, and the breaking C−C bonds.

isomers of **VII′**OH, this paper presents no further discussions of (*E*)-**VII′**OH or its decomposition pathways.

We now turn to the decomposition reactions of **VII′**OH. The structures of the transition states for different conformers of **VII′**OH are shown in Figure 3, activation barriers are listed in Table 2, and the potential energy profile for the decomposition reactions is depicted in Figure 4. The product of decomposition, 3-hydroxy-2-methylpropenal, can exist in (*E*) and (*Z*) isomers:

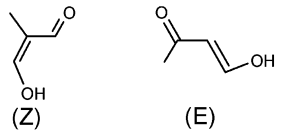

We considered eight conformers of (*Z*)- and (*E*)-3-hydroxy-2-methylpropenal with C_s symmetry, whose structures are shown in Figure 5 and relative energies are listed in Table 3. The identity of the conformer of 3-hydroxy-2-methylpropenal that forms during the decomposition of a molecule of **VII′**OH depends on which conformer of **VII′**OH is decomposing. For example, the (*Z*) isomer of 3-hydroxy-2-methylpropenal can possess an intramolecular hydrogen bond if the dihedral angles HOC═C and C═C−C═O are both near zero (conformer #2); this hydrogen bond correlates to the (3→1) hydrogen bond of **VII′**OH. Therefore, the decomposition of (*Z*)-**VII′**OH (3→1) and (*Z*)-**VII′**OH (4→3,3→1) produces conformer #2 of 3-hydroxy-2-methylpropenal. All other conformers of (*Z*)-**VII′**OH decompose to form conformers #3 or #6 of 3-hydroxy-2-methylpropenal. As shown by the data in Table 3, conformer #2 is the most stable, by 8.7 kcal/mol over #3, which is only 0.5 kcal/mol more stable than #6.

TABLE 2: Activation Barriers (kcal/mol) at B3LYP for 1,5 H-shift, E/Z Isomerization, Decomposition, and Other Reactions of VIIO and VII′OH

reaction	6-31G-(d,p)	6-311G-(2df,2p)
(*Z*)-**VII**O (1→4) → (*Z*)-**VII**O (1→3)	5.8	5.6
(*Z*)-**VII**O (1→3) → (*Z*)-**VII′**OH (4→3,3→1)	−0.3	0.3
(*Z*)-**VII**O (1→3)′ → (*Z*)-**VII′**OH (4→3,3→1)	−1.8	−1.4
(*Z*)-**VII**O (1→3)′ → decomposition[b]	−2.6	−3.5
(*Z*)-**VII′**OH (4→3,3→1) → decomposition[a,b]	18.9	17.6
(*Z*)-**VII′**OH (4→1) → decomposition[a,c]	20.6	19.1
(*Z*)-**VII′**OH (3→1) → decomposition[b]	18.1	16.9
(*Z*)-**VII′**OH (4→3) → decomposition[a,c]	26.9	24.8
(*Z*)-**VII′**OH (none) → decomposition [d]	29.9	23.9
(*Z*)-**VII′**OH (none) → (*E*)-**VII′**OH (none)	22.7	22.4
(*Z*)-**VII′**OH (3→4) →(*E*)-**VII′**OH (3→4)	16.0	15.8
(*Z*)-**VII′**OH (4→3) → (*E*)-**VII′**OH (4→3)	17.8	17.5
(*E*)-**VII′**OH (none) → decomposition[e]	20.5	18.8
(*E*)-**VII′**OH (4→3) → decomposition[a,f]	25.4	23.1
(*Z*)-**VII′**OH (none) → (1,5 H-shift)	24.8	25.3

[a] Direct product is an exit channel complex. [b] Produces conformer #2 of 3-hydroxy-2-methyl-2-propenal. [c] Produces conformer #6 of 3-hydroxy-2-methyl-2-propenal. [d] Produces conformer #3 of 3-hydroxy-2-methyl-2-propenal. [e] Produces conformer #4 of 3-hydroxy-2-methyl-2-propenal. [f] Produces conformer #5 of 3-hydroxy-2-methyl-2-propenal.

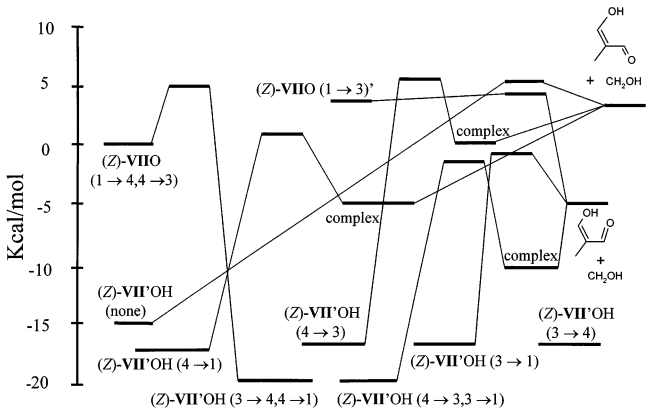

Figure 4. Potential energy profile for decomposition reactions of **VII′**OH. Various exit channel complexes between 3-hydroxy-2-methyl-2-propenal and •CH_2OH are identified generically as "complex".

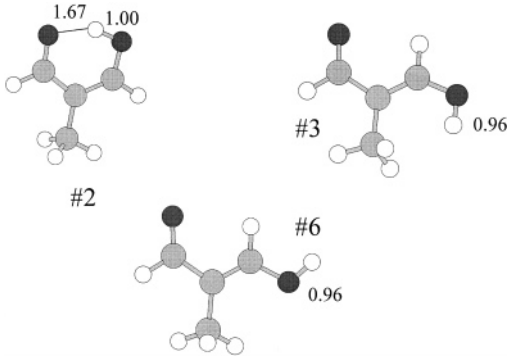

Figure 5. Structures of conformers of 3-hydroxy-2-methyl-2-propenal formed as products of the decomposition reactions of **VII′**OH. O−H distances (B3LYP/6-311G(2df,2p) values, in Å) are listed for covalent bonds and hydrogen bonds.

The barrier heights for the decomposition are lower for reactions forming the more stable (hydrogen bonded) product, as indicated in Table 2 and shown in Figure 4. Exit channel

TABLE 3: Relative Energies (kcal/mol) at B3LYP/6-31G(d,p) of Isomers and Conformers of 3-hydroxy-2-methylpropenal, the Product of Decomposition of VII′OH[a]

conformer	*E* or *Z*	HOC=C	C=C−C=O	energy
1	*Z*	0	180	9.7
2	*Z*	0	0	0.0
3	*E*	0	0	8.7
4	*E*	0	180	6.4
5	*E*	180	180	7.8
6	*E*	180	0	9.2
7	*Z*	180	0	14.6
8	*Z*	180	180	10.3

[a] Only conformer #2 can possess an intramolecular hydrogen bond.

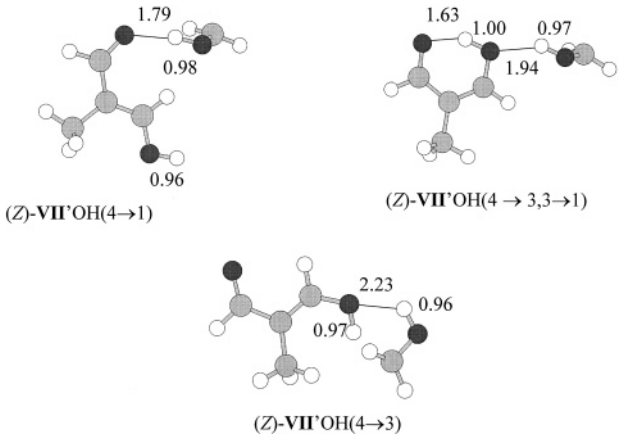

Figure 6. Structures of exit channel complexes formed in the decomposition reactions of various conformers of **VII′**OH. Complexes are identified by the structure of the reactant. O−H distances (B3LYP/6-311G(2df,2p) values, in Å) are listed for covalent bonds and hydrogen bonds.

complexes can also form when the $^{\bullet}CH_2OH$ radical leaving group donates a hydrogen bond to one of the oxygen atoms of 3-hydroxy-2-methylpropenal (see Figure 6). Energies of the exit channel complexes are listed in Table 1. Note that we were unable to find a transition state for the decomposition of **VII′**OH (3→4) or **VII′**OH (3→4,4→1) to 3-hydroxy-2-methylpropenal.

The internal hydrogen abstraction reaction of **VII′**OH is analogous to the 1,5 H-shift (isomerization) of alkoxy radicals:

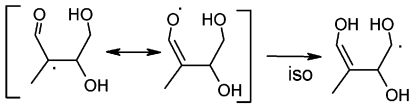

(5)

However, the transition state for this reaction lies 29.5 kcal/mol above **VII′**OH (3→4,4→1), and reaction 5 is therefore unimportant. While other (1,*n*) H-shift reactions could be imagined, they would presumably be less favorable due to increased ring strain in their transition states.

B. Kinetic Modeling. We constructed a kinetic model in MultiWell[5] to determine the extent to which **VII′**OH promptly decomposes in competition with quenching. The simulation considers one molecule at a time, starting as (*Z*)-**VII**O (1→4,4→3); a total of 10 000 molecules were examined. The initial energy of the molecule is set to a specific (elevated) energy or randomly set according to a 298 K Boltzmann probability distribution. At each time step, the molecule may undergo collisional energy exchange with the N_2 bath gas, or could be transformed to a different conformer or decomposition product in accord with the probability of that process. The full model included all conformers of (*Z*)-**VII**O, (*Z*)-**VII′**OH, and (*E*)-**VII′**OH with zero, one, and two hydrogen bonds, as well as the exit channel complexes. All decomposition reactions of the **VII′**OH conformers were included, as was the decomposition of (*Z*)-**VII**O (1→3) and (*Z*)-**VII**O (1→3)′ (see ref 1) and the 1,5 H-shift of (*Z*)-**VII′**OH (which was set to be allowed for each conformer). The energies of the decomposition products were taken either to be that of #2 (the hydrogen-bonded conformer) or #3 (for the non-hydrogen-bonded products); the small energy difference between conformers #3 and #6 was neglected for modeling purposes. Since the non-hydrogen-bonded products were always less than 2% of the total yield of decomposition product, this simplification should have a negligible effect on computed yields. The rearrangements of (*Z*)-**VII**O (1→4) to (*Z*)-**VII**O (1→3) and (*Z*)-**VII**O (1→3)′ were also included (assuming identical barrier heights). All the reactions listed above were treated with standard transition state theory. Reactions were studied at 300 K and either 10 or 760 Torr of N_2 bath gas, to provide information relevant to both laboratory and atmospheric conditions. Tunneling effects on the rate constant for the intramolecular H-atom transfer reactions were neglected, as there was no convenient way to include them in the model.

Two types of processes occur in these simulations for which transition states are not well-defined. One of these is the conformational changes involved in the breaking and forming of hydrogen bonds among conformers of **VII′**OH and **VII**O. We made several unsuccessful attempts to find transition states for the rearrangements of the hydrogen bonding that interconvert conformers of (*Z*)-**VII′**OH. However, these rearrangements are qualitatively different from, for example, the decomposition reactions, where the breaking of a covalent C−C bond occurs in concert with formation of a C=C π bond. The breaking of one hydrogen bond and formation of a different one are generally not concerted events, in which case the transformation of, e.g., **VII′**OH (3→4) to **VII′**OH (3→1) is properly treated as a two-step process: **VII′**OH (3→4) → **VII′**OH (none) followed by **VII′**OH (none) → **VII′**OH (3→1). If there was a saddle point connecting these two conformers, it would occur on a very flat potential energy surface and be close in energy to the conformer with no hydrogen bonds. In this case, it would be very difficult to find a transition state structure, and the energetics of the process would be well-approximated by a two-step process. The one transition state we found[1] for a concerted hydrogen bond fission/formation event (namely, (*Z*)-**VII**O (1→4) → (*Z*)-**VII**O (1→3)) was not unambiguously identified as such, and was only 0.4 kcal/mol lower in energy than (*Z*)-**VII**O (none). Therefore, except for (*Z*)-**VII**O (1→4) → (*Z*)-**VII**O (1→3), we only considered conformational interconversions in which a single hydrogen bond was broken or formed. For these reactions, we assumed an activation barrier of 1.0 kcal/mol (above the higher lying conformer).

It is also necessary to model the rate of decomposition of exit channel complexes to separated products. We assumed the absence of a barrier to the decomposition of exit channel complexes other than the computed binding energy of the complex. The computed binding energies of the exit channel complexes reported here are not corrected for basis set superposition error (BSSE), which is the tendency of binding energies to be overestimated when using finite basis sets. Test calculations in MultiWell determined that the fate of the exit channel complexes was, in over 99% of trials, decomposition to separated products rather than back-reaction to **VII′**OH.

Correcting the binding energies for BSSE would further increase the rate of decomposition to separated products, which would have a negligible effect on the product yields determined in our simulations. Therefore, the neglect of BSSE in the simulations is justified.

To estimate microcanonical rate constants for decomposition of exit-channel complexes and conformational interconversions, we turned to the inverse LaPlace transform:[9]

$$k(E) = A_\infty \frac{N(E - E_o)}{N(E)} \quad (6)$$

where $N(E)$ and $N(E - E_o)$ are the densities of states of the *reactant* computed at energies differing by the (zero-point corrected) barrier height. Essentially, the density of states of a transition state is approximated by that of the reactant, shifted by the barrier height. This also requires specification of a value for the high-pressure limiting value of the Arrhenius preexponential factor, A_∞. A value of 10^{13} s^{-1} was assumed both for hydrogen bond breaking/forming and for decomposition of the exit channel complexes into isolated products.

Two series of calculations were carried out to determine how sensitively the extent of prompt decomposition of **VII′**OH depended on the assumed values of A_∞ and E_o for conformational interconversion. Calculations were carried out at six initial energies with an assumed barrier of 3.0 kcal/mol instead of 1 kcal/mol for the hydrogen bond breaking, but the resulting changes in the extent of prompt decomposition were less than the statistical uncertainty in 4 out of the 6 cases. In four other simulations, we used $A_\infty = 10^{11}$ s^{-1} and an activation barrier of 3.0 kcal/mol for breaking of hydrogen bonds. In three of these four cases the extent of prompt decomposition was within one standard deviation of the previous results. Therefore, these parameters were not a significant source of the uncertainty. This makes sense, since as long as the rates of conformational interconversion are significantly faster than the rates of decomposition, the relative populations of the conformers are expected to be in pseudoequilibrium.

Recall that the goal of these simulations was to determine the extent of prompt decomposition of energized **VII′**OH. Prompt decomposition is distinguished from thermal reaction by the time scale on which it occurs: faster than quenching to thermal energies. For purposes of this analysis, prompt decomposition of **VII′**OH was considered to have finished when all **VII**O radicals had reacted and all the resulting **VII′**OH radicals were either decomposed or quenched to energies below the activation barrier to their decomposition. At the temperatures and pressures of interest here, this occurred on a time scale much shorter than that for thermal (298 K) reaction.

Having validated or, at least, rationalized the details of the model, we can now begin to consider the results. When (*Z*)-**VII**O (1→4,4→3) was initialized at a 300 K distribution of energy and the B3LYP/6-311G(2df,2p) activation energy for double H-atom transfer is used, no decomposition occurred. Even with use of the higher computed activation barrier[1] for the double H-atom transfer from MPW1K (which implies more energized **VII′**OH radicals than does the B3LYP result) there is only a 1.7% yield of decomposition products. However, under polluted conditions alkoxy radicals are expected to be formed with considerable excess energy, leading to the possibility of more extensive decomposition.[10−16] Figure 7 shows the yield of prompt decomposition product at 10 and 760 Torr of N_2 versus the initial energy of the alkoxy radical. Isomerization (reaction 5) was never observed, even at the highest energies employed in the simulations.

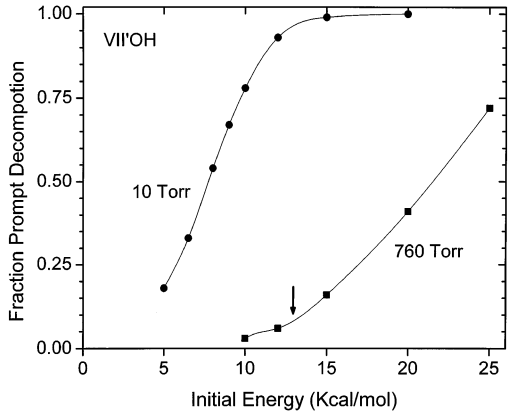

Figure 7. Fraction of **VII′**OH promptly decomposing to 3-hydroxy-2-methyl-2-propenal + $^\bullet CH_2OH$ as a function of initial energy of **VII**O at 10 and 760 Torr. Lines are merely guides to the eye. The arrow indicates the average energy of a molecule of **VII**O produced in the **VII**OO + NO reaction.

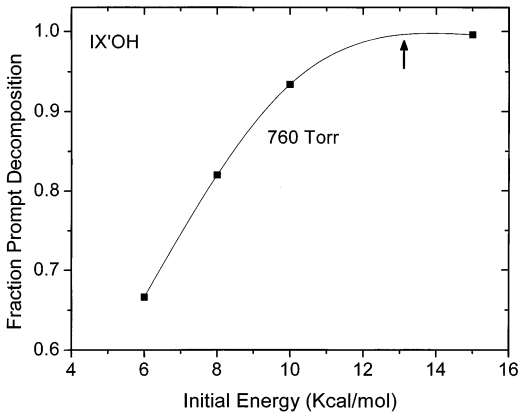

Figure 8. Fraction of **IX′**OH promptly decomposing to 3-hydroxy-2-butenal + $^\bullet CH_2OH$ as a function of initial energy of **IX**O at 760 Torr. Lines are merely guides to the eye. The arrow indicates the average energy of a molecule of **IX**O produced in the **IX**OO + NO reaction.

The simulations indicate that when prompt decomposition occurred, the hydrogen bonded conformer (#2) of 3-hydroxy-2-methylpropenal was almost the sole product (>98%). Even though decomposition of **VII′**OH yields a distribution of conformers of (*Z*)-3-hydroxy-2-methylpropenal different from that expected at equilibrium, the populations of conformers will attain thermal equilibrium on a time scale much shorter than that required for further chemical transformation. Therefore, we report only total yields of product and do not report yields of specific conformers.

If the initial energy distribution was known then the overall fraction of prompt decomposition could be determined from Figure 8. The Separate Statistical Ensemble theory (SSE)[17] has been used several times to estimate the initial energy distribution of alkoxy radicals formed in the ROO + NO reaction,[16,18−20] although there is no direct evidence for the validity of SSE in this situation. We have not carried out the necessary calculation, but provide some estimates here based on the results of previous applications of SSE to chemically activated alkoxy radicals. Specifically, the distribution of energy available to the alkoxy radical can be well-approximated as a symmetric distribution centered about an energy of[16,18−20]

$$\Delta H_r \frac{n_{RO}}{n_{RO} + n_{NO_2}} \quad (7)$$

TABLE 4: B3LYP Energies (kcal/mol) of IXO, IX′OH, Their Conformers and Isomers, and the Decomposition Products of IX′OH, Relative to (*Z*)-IX′OH (3→4,4→1)

species	B3LYP/ 6-31G(d,p)	B3LYP/ 6-311G(2df,2p)
(*Z*)-**IX**O (1→4,4→3)	14.8	15.3
(*E*)-**IX**O (4→3)	22.7	22.2
(*Z*)-**IX**O (1→4)	22.4	21.7
(*Z*)-**IX**O (4→3)	29.8	28.3
(*Z*)-**IX′**OH (3→4,4→1)	0	0
(*Z*)-**IX′**OH (4→3,3→1)	0.7	0.2
(*Z*)-**IX′**OH (3→1)	7.3	5.7
(*Z*)-**IX′**OH (4→1)	2.9	1.9
(*Z*)-**IX′**OH (3→4)	4.2	3.1
3-hydroxy-2-butenal (H-bonded conformer) + CH_2OH	9.5	5.8

TABLE 5: Activation Barriers (kcal/mol) at B3LYP for Decomposition Reactions of IX′OH

reaction	6-31G(d,p)	6-311G(2df,2p)
(*Z*)-**IX′**OH (none) → product	26.1	23.1
(*Z*)-**IX′**OH (3→1) → product	23.8	22.0
(*Z*)-**IX′**OH (4→3,3→1) → product	13.3	11.5
(*Z*)-**IX′**OH (4→1) → product	15.6	13.4

where n_{RO} and n_{NO_2} are the number of vibrational modes of the alkoxy radical and of NO_2, respectively (this approximation likely fails at higher temperatures). The value of $\Delta H_r(0\ K)$ for (*Z*)-**VII**OO (1→4,4→3) + NO → (*Z*)-**VII**O (1→4,4→3) + NO_2 is 14.2 kcal/mol at 0 K with use of the CBS-QB3 level of theory.[1] This implies that the average energy of a **VII**O radical is ∼13 kcal/mol. As can be seen from Figure 7, relatively little of the **VII′**OH undergoes prompt decomposition at this energy, and the dominant fate is quenching (at 760 Torr of N_2 at 298 K). However, at a total pressure of 10 Torr it requires an initial energy of only 8 kcal/mol to ensure prompt decomposition of 50% of **VII′**OH.

We now turn our attention briefly to the fate of the **IX′**OH radicals formed from the alkoxy radical **IX**O. Relative energies of conformers of **IX′**OH, where calculated, are listed in Table 4, and activation barriers are listed in Table 5. The exothermicity (at 0 K) of the double H-atom transfer of **IX**O is only 15.3 kcal/mol compared to 19.2 kcal/mol in **VII**O, and the lowest barriers to decomposition of **IX′**OH (from the (4→3,3→1) and (3→1) conformers of **IX′**OH to hydrogen-bonded 3-hydroxy-2-butenal) are only 11.5 and 13.4 kcal/mol (versus ∼17 kcal/

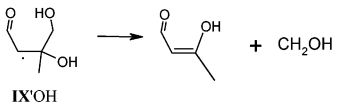

IX'OH (8)

mol in **VII′**OH). The combination of the lower well-depth and a lower barrier to decomposition in **IX′**OH versus **VII′**OH implies that prompt decomposition will be more extensive in **IX′**OH than in **VII′**OH. Thermal decomposition of **IX′**OH ($k \sim 10^5\ s^{-1}$ at 298 K and 1 atm of N_2) is 10 000 times faster than that of **VII′**OH, and might compete with reaction with O_2 in 1 atm of air (expected pseudo-first-order rate constant $\sim 5 \times 10^6\ s^{-1}$).[23] The 1,5 H-shift reaction was assumed to be unimportant, by analogy to our finding for **VII′**OH.

The potential energy surface for **IX′**OH is presumably as complicated as that for **VII′**OH. To avoid having to characterize all the conformers, isomers, transition states, and exit-channel complexes for the **IX′**OH reaction system, and to avoid calculating the densities of states of all the relevant species, an approximate model is employed in place of the detailed model used for **VII′**OH. By analogy to **VII′**OH, it is assumed that the only significant reaction pathways are decomposition via reaction 8 to produce *hydrogen-bonded* conformers of the product, as discussed in the previous paragraph. This permits use of approximate treatments of all other reactions without introducing significant error. Another time savings was achieved by using the densities of states of the species from the **VII′**OH potential energy surface for simulations of the **IX′**OH system. This is reasonable in light of the close similarity of these two isomers. The structures and energies of the transition states for decomposition of **IX′**OH (from the (4→3,3→1) and (3→1) conformers) were determined (Table 5) at B3LYP/6-311G(2df,-2p) with zero-point energies at B3LYP/6-31G(d,p), as were the energies of the relevant conformers of **IX′**OH (Table 4). Relative energies that were not explicitly calculated were taken to equal those obtained in the **VII′**OH system.

The results confirm that **IX′**OH is much more likely than **VII′**OH to undergo prompt decomposition. Prompt decomposition is the sole fate of **IX′**OH radicals at 10 Torr, regardless of the initial energy of the radical (at least 99.9% of the time, with a statistical error of 0.03%). At 760 Torr, almost two-thirds of the **IX′**OH undergo prompt decomposition even when formed from (*Z*)-**IX**O (1→4,4→3) initially possessing a Boltzmann distribution of energy. Note that formation of (*Z*)-**IX**O (1→4,4→3) has $\Delta H_r(0K) = -14.1$ kcal/mol. With use of our approximation of the Separate Statistical Ensemble theory, described above, the average **IX**O molecule is formed with ∼13 kcal/mol of energy. As shown in Figure 8, the fraction of molecules undergoing prompt decomposition rises to 93% when radicals are formed with an initial energy of 10 kcal/mol. Therefore, decomposition appears to be the overwhelmingly dominant fate of **IX′**OH under polluted atmospheric conditions.

Let us consider the uncertainty in the model predictions of the fraction of prompt decomposition of **VII′**OH. Major sources of error arise primarily from errors in the computed values of the exothermicity of the double H-atom transfer and the heights of the lowest activation barriers to decomposition of **VII′**OH. If the reaction were to be more exothermic than calculated, or the barrier heights to decomposition higher than calculated, the extent of prompt decomposition might be significantly less than found here. The model for prompt decomposition of **IX′**OH was more approximate than that for **VII′**OH, but the key variables were equally well determined. The greater extent of prompt decomposition in **IX′**OH than in **VII′**OH inferred from the MultiWell calculations agrees with expectations based on the qualitative arguments presented above.

Finally, we note that an assumption of the above analyses is that the various hydrogen-bonding arrangements of **VII′**OH and **IX′**OH represent distinct species which interconvert in a manner consistent with RRKM theory. Recent work has pointed out cases where non-RRKM behavior plays a major role in the dynamics of reactions where hydrogen bond formation competes with chemical reaction.[21,22] It would be interesting to search for similar non-RRKM behavior in these system.

C. Atmospheric Implications. Consider the fate of the **VII′**OH radical. The modeling results presented above suggested that most of the **VII′**OH radicals will be quenched under atmospheric conditions. The fate of the quenched **VII′**OH radicals will be reaction with O_2 (pseudo-first-order rate constant $\sim 5 \times 10^6\ s^{-1}$),[23] since the 16.9 kcal/mol barrier to decomposition renders the thermal decomposition rate slow ($\sim 10\ s^{-1}$)). This may be followed by a series of reactions leading to formation of methylglyoxal (MGLY) and glycolaldehyde as shown in Scheme 1.

SCHEME 1

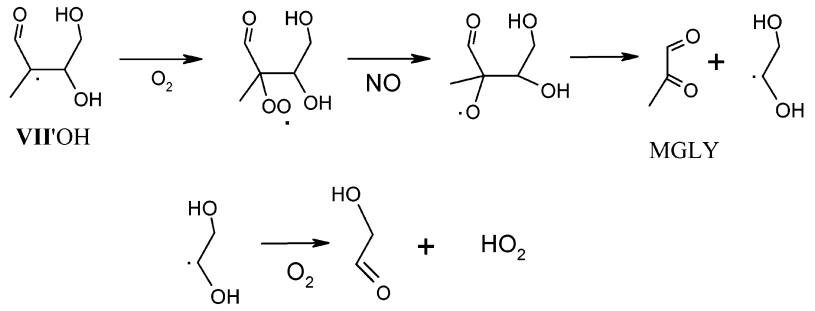

SCHEME 2

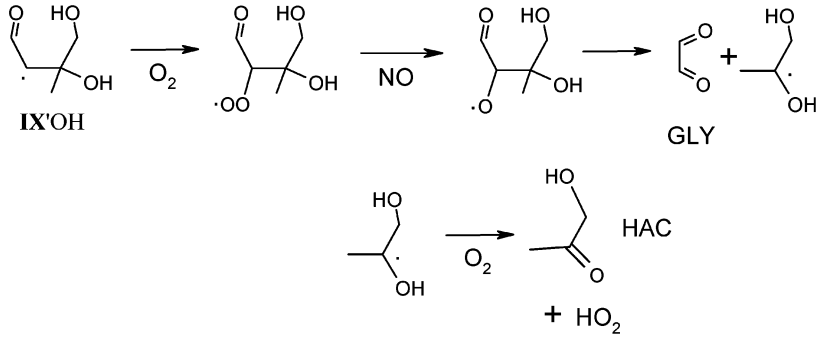

The analogous products from bimolecular reaction of thermalized **IX′**OH are expected to be glyoxal (GLY) and hydroxyacetone (HAC), via Scheme 2, below.

Glyoxal, methylglyoxal, glycolaldehyde, and hydroxyacetone have been observed previously as products of the OH-initiated degradation of isoprene in smog chamber experiments, but their formation was attributed to the secondary chemistry of the major products of isoprene.[24] The present results do not falsify that suggestion, but do suggest an alternative or additional path for their formation. Note that decomposition of either **IX**O (reaction 2 in ref 1) or **IX′**OH (reaction 8) yields $^{\bullet}CH_2OH$ radical plus $C_4H_6O_2$ unsaturated hydroxy-substituted carbonyl compounds.

Let us consider the consequences of this chemistry for ozone formation in the atmosphere. Most of the **IX′**OH will decompose promptly, leading to an isomer of the product that had been expected[25] from β-scission of **IX**O, whereas prompt decomposition of **VII′**OH leads to the identical product as had been expected[25] from β-scission of **VII**O. Therefore, prompt decomposition will have little effect on atmospheric chemistry. The greater part of **VII′**OH and a modest fraction of **IX′**OH will react as indicated in Schemes 1 and 2. This leads to one more NO-to-NO_2 conversion than had been expected, which creates the potential for greater ozone production than had been expected. Given the small overall yields of quenched **VII**O and **IX**O, any increases in ozone production resulting from their reactions will be small. Much greater uncertainties in ozone production arise from our ignorance of the branching ratio for formation of hydroxyl-isoprene nitrates in RO_2 + NO reactions[26] and from the challenges in determining isoprene emissions.[27,28]

Conclusions

The double H-atom transfer in second-generation alkoxy radicals from isoprene produces alkenoxy radicals **VII′**OH and **IX′**OH at elevated energies. The fates of these radicals are controlled by the competition between quenching and prompt decomposition. When **VII′**OH is formed from **VII**O radicals initially at thermal energies at 760 Torr of N_2, quenching is the sole fate of **VII′**OH. In contrast, **IX′**OH formed under similar conditions mostly undergoes prompt decomposition. Prompt decomposition will be enhanced when **VII′**OH is formed at lower pressures or from energized **VII**O (produced by **VII**OO + NO under polluted conditions), but quenching is expected to dominate under atmospherically relevant conditions. For **IX′**OH, lower pressures and higher energies cause prompt decomposition to be overwhelmingly dominant. Where prompt decomposition of the alkenoxy radicals occurs, the reaction products are essentially identical with those expected from the previously hypothesized decomposition of the alkoxy radical; therefore, this chemistry only affects the atmosphere to the extent the alkenoxy radicals are stabilized. The increase in ozone production arising from this chemistry is small in comparison to other sources of uncertainty in ozone production from isoprene.

Acknowledgment. This research was supported by the National Science Foundation under grant ATM0087057 and the National Computational Science Alliance under grant ATM010-003N, utilizing the HP-N4000 cluster at the University of Kentucky. The author thanks J. R. Barker for assistance with the MultiWell program, and K. Kitney, L. Zhang, and two anonymous referees for their extensive comments on the manuscript.

Supporting Information Available: Cartesian coordinates of radicals and transition states at B3LYP/6-311G(2df,2p), together with absolute energies of radicals and transition states. This material is available free of charge via the Internet at http://pubs.acs.org.

References and Notes

(1) Dibble, T. S. *J. Phys. Chem. A* **2004**, *108*, 2199.

(2) Frisch, M. J.; Trucks, G. W.; Schlegel, H. B.; Scuseria, G. E.; Robb, M. A.; Cheeseman, J. R.; Zakrzewski, V. G.; Montgomery, J. A., Jr.; Stratmann, R. E.; Burant, J. C.; Dapprich, S.; Millam, J. M.; Daniels, A. D.; Kudin, K. N.; Strain, M. C.; Farkas, O.; Tomasi, J.; Barone, V.; Cossi, M.; Cammi, R.; Mennucci, B.; Pomelli, C.; Adamo, C.; Clifford, S.; Ochterski, J.; Petersson, G. A.; Ayala, P. Y.; Cui, Q.; Morokuma, K.; Malick, D. K.; Rabuck, A. D.; Raghavachari, K.; Foresman, J. B.; Cioslowski, J.; Ortiz, J. V.; Stefanov, B. B.; Liu, G.; Liashenko, A.; Piskorz, P.; Komaromi,

I.; Gomperts, R.; Martin, R. L.; Fox, D. J.; Keith, T.; Al-Laham, M. A.; Peng, C. Y.; Nanayakkara, A.; Gonzalez, C.; Challacombe, M.; Gill, P. M. W.; Johnson, B.; Chen, W.; Wong, M. W.; Andres, J. L.; Gonzalez, C.; Head-Gordon, M.; Replogle, E. S.; Pople, J. A. *Gaussian 9*8, Revision A.6; Gaussian, Inc.: Pittsburgh, PA, 1998.

(3) Becke, A. D. *J. Chem. Phys.* **1993**, *98*, 5648.

(4) Lee, C.; Yang, W.; Parr, R. G. *Phys. Rev. B* **1988**, *37*, 785.

(5) Barker, J. R. MultiWell software, version 1.3.1, 2003.

(6) Barker, J. R. *Int. J. Chem. Kinet.* **2001**, *33*, 232.

(7) Gilbert, R. G.; Smith, S. C. *Theory of Unimolecular and Recombination Reactions*; Blackwell Scientific: Oxford, UK, 1990; p 318.

(8) Barker, J. R.; Yoder, L. M.; King, K. D. *J. Phys. Chem.* **2001**, *105*, 796.

(9) Forst, W. J. *J. Phys. Chem.* **1983**, *83*, 100.

(10) Orlando, J. J.; Tyndall, G. S.; Bilde, M.; Ferronato, C.; Wallington, T. J.; Vereecken, L.; Peeters, J. *J. Phys. Chem. A* **1998**, *102*, 8116.

(11) Wallington, T. J.; Hurley, M. D.; Maurer, T.; Barnes, I.; Becker, K. H.; Tyndall, G. S.; Orlando, J. J.; Pimentel, A. S.; Bilde, M. *J. Phys. Chem. A* **2001**, *105*, 5146.

(12) Orlando, J. J.; Tyndall, G. S.; Vereecken, L.; Peeters, J. *J. Phys. Chem. A* **2000**, *104*, 11578.

(13) Park, J.; Stephens, J. C.; Zhang, R.; North, S. W. *J. Phys. Chem. A* Submitted for publication.

(14) Lei, W.; Zhang, R. *J. Phys. Chem. A* **2001**, *105*, 3808.

(15) Dibble, T. S. *J. Phys. Chem. A* **1999**, *103*, 8559.

(16) Zhao, J.; Zhang, R.; North, S. W. *Chem. Phys. Lett.* **2003**, *369*, 204.

(17) Wittig, C.; Nadler, I.; Reisler, H.; Noble, M.; Catanzarite, J.; Radhakrishnan, G. *J. Chem. Phys.* **1985**, 83, 5581.

(18) Vereecken, L.; Peeters, J. *J. Phys. Chem A* **1999**, *103*, 1768.

(19) Vereecken, L.; Peeters, J.; Orlando, J. J.; Tyndall, G. S.; Ferronato, C. *J. Phys. Chem. A* **1999**, *103*, 4693.

(20) Caralp, F.; Forst, W.; Rayez, M.-T. *Phys. Chem. Chem. Phys.* **2003**, *5*, 476.

(21) Sun, L.; Song, K.; Hase, W. L. *Science* **2002**, *296*, 875.

(22) Wang, Y.; Hase, W. L.; Wang, H. *J. Chem. Phys.* **2003**, *118*, 2688.

(23) Based on present knowledge of the rate constants for other alkenoxy radicals extracted from the NIST Standard Reference Database 17, Version 7.0. $k_{O_2} \sim 1 \times 10^{-12}$ cm^3 molecule^{-1} s^{-1}.

(24) Yu, J.; Jeffries, H. E.; Le Lacheur, R. M. *Environ. Sci. Technol.* **1995**, *29*, 1923.

(25) Paulson, S. E.; Seinfeld, J. H. *J. Geophys. Res.* **1992**, *97*, 20703.

(26) Poschl, U.; von Kulmann, R.; Poisson, N.; Crutzen, P. J. *J. Atmos. Chem.* **2000**, *37*, 29.

(27) Geron, C.; Harley, P.; Guenther, A. *Atmos. Environ.* **2001**, *35*, 3341.

(28) Guenther, A. B.; Zimmerman, P. R.; Harley, P. C.; Monson, R. K.; Fall, R. *J. Geophys. Res.* **1993**, *98*, 12609.